Journal of Power Sources 257 (2014) 412–420

Contents lists available at ScienceDirect

Journal of Power Sources

journal homepage: www.elsevier.com/locate/jpowsour

Fuel cell–gas turbine hybrid system design part I: Steady state performance

Dustin McLarty, Jack Brouwer*, Scott Samuelsen

National Fuel Cell Research Center, University of California, Irvine, CA 92697, USA

HIGHLIGHTS

- A novel methodology for design of MCFC and SOFC gas turbine hybrids is presented.
- Off-design performance and operating envelopes are determined from physical models.
- Existing MCFC and micro-turbine technology achieves 74.4% efficiency (LHV) at 1.2 MW.
- SOFC–GT technology is shown to achieve >75% efficiency (LHV) on synthesis gas.
- Thermodynamic compatibility of FC and GT is achieved with recirculation and bypass.

ARTICLE INFO

Article history:
Received 16 August 2013
Received in revised form
25 November 2013
Accepted 29 November 2013
Available online 28 December 2013

Keywords:
Hybrid fuel cell gas turbine
Solid oxide fuel cell
Molten carbonate fuel cell
System design
Performance matching
Efficiency

ABSTRACT

The hybridization of gas turbine technology with high temperature fuel cells represents an ultra-high efficiency, ultra-low emission, fuel flexible power generation platform. The performance of past prototypes has been limited by marginal compatibility of the two primary sub-systems. This paper addresses the challenge of selecting compatible hardware by presenting a simple and robust method for bespoke hybrid system design and off-the-shelf component integration. This is the first application of detailed, spatially resolved, physical models capable of resolving off-design performance to the integration analysis of FC–GT hybrids. Static maps are produced for both turbine and fuel cell sub-systems that readily evaluate the compatibility and hybrid performance. Molten carbonate and solid oxide fuel cells are considered for hybridization with recuperated micro-turbines and larger axial flow gas turbine systems. Current state-of-the-art molten carbonate technology is shown to pair well with present micro-turbine technology in an FC bottoming cycle design achieving 74.4% LHV efficiency. Solid oxide technology demonstrates remarkable potential for integration with larger scale axial turbo-machinery to achieve greater than 75% LHV efficiency. This performance map technique closely matches results from detailed integrated hybrid system analyses, and enables quick determination of performance requirements for balance of plant design and optimization.

1. Introduction

Integration of fuel cell and gas turbine technologies into a single symbiotic hybrid system has been shown to produce systems with high fuel-to-electricity conversion efficiency [1–4]. Fuel cell–gas turbine hybrids (FC–GT) have the potential for ultra-high efficiency, ultra-low emissions, fuel flexibility, and dynamic responsiveness [5,6]. In addition, such hybrid systems scale easily and have an inherent advantage in CO_2 separation for carbon capture and sequestration/utilization [7–9].

The integration of fuel cell systems with gas turbine systems provides an opportunity to exploit synergies of integration that include conversion of waste heat to additional electricity and compression power, fuel cell pressurization that increases efficiency, and air pre-heating. A fuel cell extracts work directly from the chemical energy of a fuel, producing much less entropy than a combustion process. This allows efficient electrical generation, but electrochemical losses, internal resistance and post-anode fuel oxidation generate substantial amounts of high temperature heat that is capable of powering a wide range of bottoming cycle engines such as gas turbines, steam turbines and Stirling engines. This

* Corresponding author. Tel.: +1 949 824 1999; fax: +1 949 824 7423.
E-mail addresses: jb@nfcrc.uci.edu, jb@apep.uci.edu, jbrouwer@uci.edu (J. Brouwer).

0378-7753/$ – see front matter © 2014 Elsevier B.V. All rights reserved.
http://dx.doi.org/10.1016/j.jpowsour.2013.11.122

Nomenclature

b	fuel cell bypass
FC	fuel cell
GT	gas turbine
MTG	micro-turbine generator
η	efficiency
$\dot{Q}_{FC}$	total fuel cell heating
$\dot{Q}_{GT}$	total combustion heating
$\hat{q}_{FC}$	specific fuel cell heating
$\hat{q}_{GT}$	specific combustion heating
r	cathode recirculation
T	temperature
U_{fuel}	fuel utilization
$\dot{w}$	specific power

paper presents a strategy for the design of a fuel cell gas turbine hybrid using bespoke or off-the-shelf systems. Additionally the methodology provides valuable insights regarding net electrical efficiency, balance of plant requirements, and potential operating envelope of the integrated system.

The waste heat generated by solid oxide and molten carbonate fuel cells is of sufficient quality, i.e., temperature, to produce additional electricity and compression power from a gas turbine in a hybrid FC–GT configuration. The fuel cell can be placed either upstream of the turbine in what is known as a topping cycle, or downstream of the turbine in a bottoming cycle. The parasitic blower load, amounting to as much as 15% of the rated fuel cell output, is avoided through integration with the turbine air flow. Placing the fuel cell in a high pressure section between the compressor and turbine benefits the fuel cell efficiency by increasing reactant partial pressures and lowering some polarization terms. This topping-cycle design introduces the need for a pressure vessel and increases the potential for compressor stall/surge. In both topping and bottoming cycles the turbine can provide a substantial portion of the air pre-heating requirement for the fuel cell, either through compression, recuperation, or recirculation. This function of the turbo-machinery can replace a portion of the fuel cell balance of plant that would otherwise be required for recouping fuel cell stack exhaust heat.

Realizing the ultra-high electrical efficiency potential of fuel cell gas turbine hybrids requires an analysis tool that systematically determines the compatibility of existing turbo-machinery and solid oxide or molten carbonate fuel cells (SOFC or MCFC). The performance map methodology detailed in this paper provides the basis of such a tool when off-design performance of both sub-systems can be modeled or experimentally determined. The methodology is applied to demonstrate the estimation of hybrid efficiency for two well-defined sub-systems, and to demonstrate how performance criteria can be established for a purpose designed or bespoke turbine that would meet the requirements of existing SOFC or MCFC equipment and provide for a large operating envelope.

2. Background

Hybridization of current state-of-the-art fuel cell and gas turbine technology has the potential to surpass the fuel-to-electricity efficiency and emissions performance of all presently deployed dispatchable power generation technologies across a broad range of applications and scales [10,11]. Previous investigations into various applications of fuel cell turbine hybrids including natural gas pressure reduction stations [12], advanced locomotives [13,14], biomass- [15] or biogas-fired [16] systems, and coal gasification with CO_2 sequestration [1] have yielded promising results. The literature describes systems ranging from the small distributed generation scale [2], to the intermediate micro-grid scale [3], all the way up to large coal syngas-fired central plant scale systems [1,4]. A well-considered review of the simulation and design efforts of the fuel cell turbine hybrid modeling community indicated that more than half of the publications were focused on cycle configuration analysis [17]. The United States Department of Energy has identified high temperature fuel cell turbine hybrids as a key component of FutureGen plants [18]. Considerable work has been done to illustrate the ultra-high fuel-to-electricity conversion efficiencies that hybrid systems can achieve, which is greater than 80%LHV when operating on natural gas [19].

Both solid oxide hybrids [5] and molten carbonate hybrids [20] have been successfully demonstrated in the sub-MW size class to achieve 53% and 56% LHV efficiency, respectively, when operating on natural gas. Testing and simulation facilities that utilize combustion as a proxy for the fuel cell heat generation have been constructed in the United States [21,22] and Italy [23] to identify and address specific challenges in the areas of system design and control [6,24]. The primary molten carbonate cycle design considered for commercialization and studied herein is a bottoming cycle hybrid system introduced and demonstrated at the sub-MW scale by FuelCell Energy® [25]. Alternate configurations capable of higher efficiencies and higher turbine firing temperatures have been proposed and simulated by other researchers. However, specific technical hurdles such as the need for high temperature blowers, ultra-high temperature heat exchangers, and changes to the stack cooling rate of these alternate configurations have not been sufficiently addressed [26,27]. The SOFC–GT topping cycle demonstrated by Siemens-Westinghouse® has been analyzed with different micro-turbines [28], for part-load performance [29], and for internal/external fuel reformation [30] configurations. A similar SOFC topping cycle design utilized detailed off-design turbine performance maps to demonstrate an impressive 5:1 turn down ratio, while maintaining stack operating temperatures within an acceptable range [31].

The fuel cell turbine hybrid literature has yet to fully address the often experienced incompatibility of existing fuel cell and gas turbine hardware. When integrated, one or both systems are forced to operate under off-design conditions. Traditional design methodologies have paired systems with similar levels of nominal air flow with secondary consideration of the thermal integration. Prototype systems completed the integration using a variety of heat exchangers, blowers and supplemental combustors. Utilizing nominal performance values for each of the subsystems (fuel cell, gas turbine) that are integrated into the hybrid system has resulted in gross under- or over-estimated performance. Some analyses have utilized detailed off-design turbo-machinery calculations, but assumed fixed fuel cell performance parameters when pressurizing and scaling the fuel cell system [32]. Other studies incorporate multi-dimensional fuel cell models with simplified turbine performance estimates and conduct only steady-state design analysis [33,34]. Some frameworks have been proposed that integrate both detailed fuel cell and gas turbine models, but the results are limited to a single specific design case [35]. These studies overlook important coupled interactions that occur when one or both of the sub-systems are operated under off-design conditions. The current work expands upon previous hybrid system modeling at the National Fuel Cell Research Center [6,36,37], and utilizes detailed physical models to generate off-design performance maps for both the fuel cell and the gas turbine sub-systems to produce an accurate initial estimate of integrated system efficiency and performance envelope.

2.1. Ideal FC–GT efficiency

The ideal reversible fuel cell efficiency is found by dividing the available Gibbs energy of reaction by the available enthalpy of reaction. The charge transfer ion of a high temperature fuel cell is negative; O^{2-} for solid oxide and CO_3^{2-} for molten carbonate fuel cells. The products of the electrochemical reactions are formed within the anode compartment where they mix with the unreacted fuel. High levels of reaction dilute the anode fuel concentration and impose a practical limit on fuel utilization. This practical limit to fuel electrochemical conversion, typically between 70 and 90%, proportionately reduces the efficiency as follows.

$$\eta_{FC} = \frac{\Delta G}{\Delta H} U_{fuel} \tag{1}$$

A hybrid system produces electrical power directly from the electrochemical conversion within the fuel cell and from the fuel cell heat by passing the fuel cell exhaust through a turbine–generator combination. The net heat generated by the fuel cell subsystem includes both the electrochemical heat transferred to the cathode air steam and the chemical oxidation heat of the anode tail gas oxidizer. The heat can be considered at two separate temperatures if the two streams do not mix, or a single temperature if they do This heat is the thermal energy available to drive the gas turbine portion of a hybrid system, which will be referred to as the "total fuel cell heating", and denoted as $\overbrace{Q}_{FC}$. The over-brace is used to distinguish this term from the thermal value of the fuel provided as input to the fuel cell or hybrid denoted as Q_{FC}. The thermal value of the fuel is equal to the sum of the fuel cell electrical work and the total fuel cell heating value as described in Equation (2). In an ideal hybrid the total fuel cell heating will perfectly replace the "total combustion heating" that would otherwise be provided by the combustor of the gas turbine, denoted as $\overbrace{Q}_{GT}$. Again the over-brace distinguishes this term from the total gas turbine heating which may include regeneration. As mentioned previously it is also important to match the flow rate of both the gas turbine and fuel cell sub-systems. To separate the thermal compatibility of the two sub-systems from their mass flow compatibility these total heating terms are normalized by their respective flow rates; air flow for the gas turbine and cathode flow for the fuel cell. These normalized total heating values for the fuel cell and gas turbine sub-systems will be referred to as the "specific fuel cell heating" and "specific combustion heating" terms, and denoted by $\overbrace{q}_{FC}$ and $\overbrace{q}_{GT}$, respectively.

The ideal electric efficiency of a hybrid system applies the Carnot efficiency to the ratio of total fuel cell heating and total input fuel energy and adding to this the practical fuel cell efficiency; as shown in Equation (3).

$$\overbrace{Q}_{FC} + \dot{W}_{net,FC} = Q_{FC} \rightarrow \frac{\overbrace{Q}_{FC}}{Q_{FC}} = 1 - \frac{\dot{W}_{net,FC}}{Q_{FC}} = (1 - \eta_{FC}) \tag{2}$$

$$\eta_{hybrid} = \eta_{FC} + \eta_{Carnot} \frac{\overbrace{Q}_{FC}}{Q_{FC}} = \eta_{FC} + \eta_{Carnot}(1 - \eta_{FC}) \tag{3}$$

Fig. 1 illustrates the various ideal efficiency limits for fuel cells, gas turbines, and hybrid fuel cell gas turbine systems on an HHV basis. Note the 10–15% improvement of FC–GT technology compared to both fuel cells and heat engines alone, and the minimal loss of hybrid system efficiency when 80% fuel utilization is applied. From a thermodynamic perspective the cycle offers clear advantages when compared to existing systems. What is needed is an analysis methodology that can thoroughly assess the integrated performance of SOFC or MCFC equipment with either existing or future turbo-machinery. The methodology of this paper addresses this need and offers techniques for determining the optimal operating conditions and operating envelope of the combined fuel cell and gas turbine sub-systems.

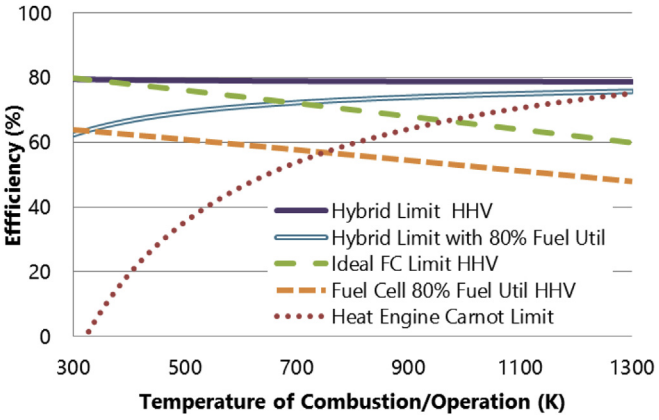

Fig. 1. Ideal efficiency comparison of fuel cells, gas turbines, and hybrids.

2.2. Modeling requirements

Detailed modeling has been employed to conduct design and performance studies that may justify further investment in FC–GT hybrid technology. Accurate simulation of FC–GT behavior that is sufficient for analysis of design requirements and determining performance characteristics and operating envelopes should contain the following characteristics.

- Physical and chemical behaviors extant each component must be resolved from first principles, with the exception of compressor and turbine components whose behavior is usually sufficiently characterized by well-established empirical maps. Detailed electrochemical and heat transfer models are necessary to capture the spatial distribution of temperature, current, and species concentrations, which are critical to fuel cell performance and operability.
- Dimensional models are superior to bulk models for their ability to capture detailed spatial information, accurate temperature and species concentration profiles, and physical behavior unrepresented by equivalent circuit models, particularly for off-design operation characterization.
- Characterization of off-design performance requires detailed understanding of the control limitations and physical constraints that may lead to degradation or failure. The absolute maximum operating envelope of both fuel cell and turbine system components must be considered during the design and system integration phase.

3. MCFC bottoming cycle

The integration of any two electric generator systems requires iterative determination of the nominal operating conditions for all components and for the design of additional balance of plant hardware. Both the fuel cell and turbine sub-systems are nominally constrained to considerably narrow operating windows. The current methodology aims to find the intersection of the operating regimes of the major sub-systems using performance maps. Data was available for two gas turbine systems that are potentially suitable for integration in small scale MCFC hybrid systems. These gas turbine sub-systems are the Garett85® turbine installed at the

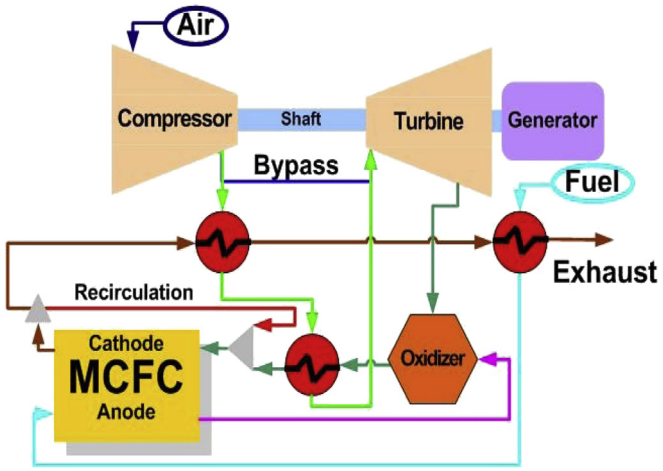

Fig. 2. MCFC bottoming cycle configuration.

National Energy Technology Laboratory (NETL) Hyper facility, and the Capstone® line of micro-turbines. Large scale hybrid systems will likely employ a larger axial flow turbine.

The requirements for molten carbonate hybridization are different from solid oxide hybridization requirements due to oxidant flow requirements (O_2 plus CO_2) for producing the transport ion (CO_3^{2-}), low operational current density, and the liquid nature of the electrolyte. Introduction of oxidized anode exhaust to the fresh air stream provides the CO_2 used to produce CO_3^{2-}. Cathode recirculation, if employed, increases the carbon dioxide concentration, benefiting the stack performance. The MCFC-bottoming cycle studied herein mixes the oxidized anode tail gas products and the indirectly heated turbine exhaust prior to the cathode inlet, see Fig. 2. The near atmospheric pressure MCFC is placed downstream of the turbine – thus the "bottoming cycle" name. The advantages of this configuration include minimal dynamic coupling of the fuel cell and turbine, reduced or eliminated air pre-heating requirements for the fuel cell, eliminated parasitic losses of an air blower, minimal modification to existing turbine hardware resulting in negligible change to stall/surge risk, and the potential for rapid dynamic response through direct firing of the turbine. The high efficiency and relatively simple controls necessary have encouraged manufacturers, FuelCell Energy® and Capstone Turbine®, to invest in demonstration prototypes. A 350 kW unit tested in Billings Montana demonstrated unprecedented 56% fuel-to-electric efficiency at this scale while operating over 8000 h with 91% availability. This analysis will demonstrate the potential for even higher efficiencies by integration of a larger Direct FuelCell® DFC-1500 MCFC with either a C-250 micro-turbine or the low-pressure spool of a C-370 turbine currently under development. Independent testing of a C-65 micro-turbine from the same Capstone-Turbine® product line was conducted at UC Irvine. The testing verified and calibrated the physical models used to generate the off-design performance maps presented in this paper.

Table 1
FuelCell energy DFC-1500 specifications.

Specification	DFC-1500	Specification	DFC-1500
Stack power (kW)	1548	Cell length (m)	1.095
Exhaust mass (lb/s)	5.083	Cell width (m)	0.8
Peak temperature (°F)	1250	Voltage (V)	0.775
Fuel utilization (%)	70.0	Current density (A m^{-2})	1600
Inverter efficiency (%)	97	Parasitic power (kW)	101.5

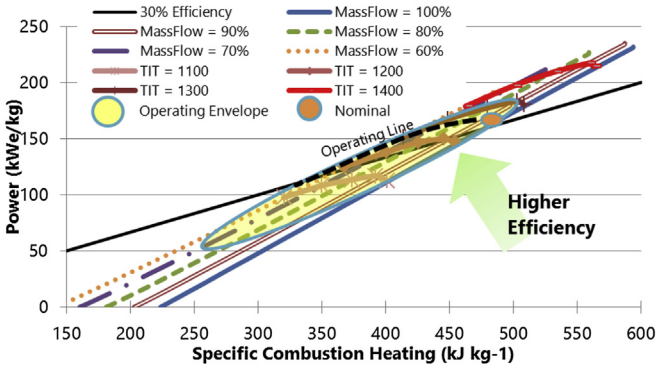

Fig. 3. Micro-turbine performance map scaled with air flow (kg s^{-1}).

This section will outline a method for determining hybrid performance of a DFC-1500 molten carbonate fuel cell, Table 1. The fuel cell is initially paired with a generic micro-turbine with the same performance characteristics of the Capstone® micro-turbine product line. Off-design operation of the physical micro-turbine models produced the performance map normalized to mass flow shown in Fig. 3. The features of this chart well represent a wide range of commercial micro-turbines. This performance map compares the specific combustion heating ($\widehat{q}_{GT}$) vs. electrical output of the micro-turbine generator (MTG). Replacing the total combustion heat with an equivalent amount of energy transfer from a fuel cell converts the MTG into an externally fired system. The nominal specific combustion heating of the micro-turbine, $\widehat{q}_{GT}$, is 479 kW s kg^{-1}.

Nominal operation of the micro-turbine can be manipulated by changing the amount of total combustion heating and the rotational speed of the turbine. Typically the fuel input controls the power output, while a load-based speed controller maintains constant exhaust temperature. Electrical output decreases with reduced total combustion heating, and the resulting speed adjustment reduces air flow to maintain operating temperature and efficiency; although some efficiency is still lost at reduced power conditions. Fig. 3 demonstrates the small operating window in which the MTG can operate. In addition to matching the mass flow rate of air, hybridization will require a specific fuel cell heating ($\widehat{q}_{FC}$) within this narrow operational window. The intersection of the specific fuel cell heating value and the turbine inlet temperature, calculated from the post-oxidation of the cathode stream, determines the turbine operating condition. The specific power of the turbine under these conditions is used in Equation (4) to find the integrated system efficiency.

Some flexibility also exists in the fuel cell operation. The controllable inputs are air flow, fuel flow, current, and operating temperature. There are considerable non-linear interactions amongst these inputs that affect the fuel cell sub-system performance. The flow rates of air, fuel, and current depend upon the size of the system. The descriptive parameters of stack temperature rise, fuel utilization, and power density can describe changes in each of the flows, respectively. A performance map similar to that of the gas turbine can be made by varying these parameters and recording the electrical and thermal output of the system to produce the results shown in Fig. 4. Note that the electrical power production, *Y*-axis, refers to the electrical output of the stack before any parasitic system loads are considered. The underlying assumption that has been applied to Equation (4) to produce these results is that all of the fuel provided to the hybrid system passes through the fuel cell, and the chemical energy stored in that fuel exits the fuel cell subsystem as either electrical power or heat, defined previously as the total fuel cell heating and given the symbol $\widehat{Q}_{FC}$.

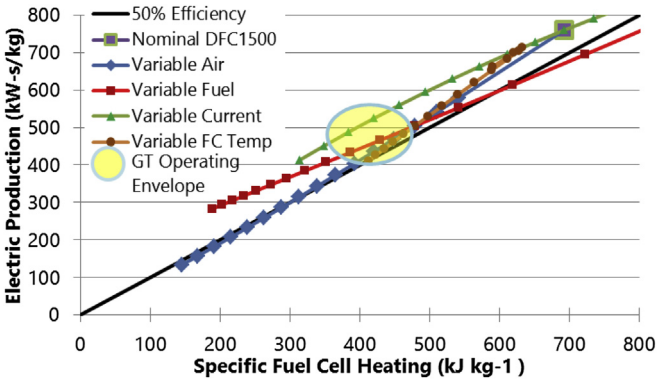

Fig. 4. Performance map for DFC-1500 molten carbonate fuel cell.

Under nominal operating conditions the specific fuel cell heating ($\widehat{q}_{FC}$) of the DFC-1500 is 692 kW s kg^{-1}. This is substantially higher than the 479 kW s kg^{-1} specific combustion heating of the micro-turbine. A portion of the excess fuel cell heat is irrevocably lost through heat transfer from the stack enclosure. The remaining difference can be lessened with several changes to the fuel cell operating conditions. The fuel cell can operate at lower current, higher air flow rate, higher fuel utilization, higher temperature or some combination of these four inputs/operating conditions. Within the small window of compatibility with the micro-turbine there is room for slight variation in each of these parameters. The objective of optimizing for system efficiency might result in slightly lower air, fuel, and current flow rates compared to those used for nominal DFC-1500 operation.

3.1. Estimating efficiency using off-design performance maps

Once the design window for integration of the fuel cell and gas turbine sub-systems has been defined, the hybrid efficiency can be estimated by adding the fuel cell and turbine electrical output, then dividing by the fuel flow times its heating value. Recalling Equation (2), which defined the thermal value of the fuel as equal to the sum of the fuel cell electrical work and the total fuel cell heating value, an expression is derived with four values that can be pulled directly from the performance maps of the individual sub-systems. The procedure for estimating the hybrid efficiency proceeds as follows:

1. Determine specific fuel cell heating and specific combustion heating values that are matched and that lie within the operating window of each sub-system
2. Select an operating condition for the fuel cell corresponding to that specific fuel cell heating value and note the specific power output of the fuel cell on the *y*-axis

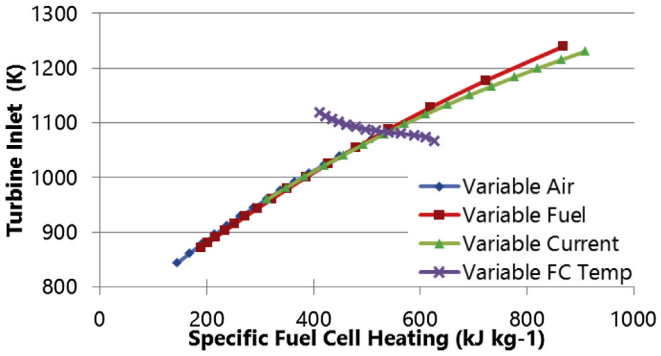

Fig. 5. Impact of fuel cell operating conditions on post-oxidizer cathode temperature.

3. Utilize the specific fuel cell heating value and the selected operating conditions to determine the maximum achievable turbine inlet temperature from a specific heating vs. temperature curve similar to that of Fig. 5
4. Find the turbine specific net power output at the intersection of the specific combustion heating value and the turbine inlet temperature determined in step 3
5. Evaluate the specific work of the turbine and fuel cell along with the specific fuel cell heating value in Equation 4

$$\eta_{hybrid} = \frac{\dot{W}_{FC} + \dot{W}_{GT}}{Q_{FC}} = \frac{\dot{W}_{FC} + \dot{W}_{GT}}{\dot{W}_{FC} + \widehat{Q}_{FC}} \quad (4)$$

Changing the operating temperature of a molten carbonate fuel cell is not feasible due to the nature of the electrolyte, nor is this desirable for a solid oxide fuel cell due to increased thermal stress and degradation at higher temperatures and increased ohmic losses at lower temperatures. It is unclear if the relatively low nominal fuel utilization of 70% for the DFC-1500 is to avoid degradation due to fuel starvation or to provide sufficient energy for cathode pre-heating. If the system can tolerate operating at higher fuel utilization, this change would be the most effective way to reduce the specific fuel cell heating to equal the specific combustion heating in the operating window of a micro-turbine. An alternative means to reduce the specific fuel cell heating would be a partial extraction of hydrogen from the anode tail gas for separate applications such as vehicle fueling in a tri-generation plant [38].

Other means of reducing the specific fuel cell heating include increasing the air flow rate or decreasing the current. Additional air flow reduces thermal gradients and the achievable turbine inlet temperature. A higher air flow rate provides additional stack cooling, necessitating additional cathode pre-heating to maintain the required fuel cell operating temperature. Recuperation could suffice if the exhaust quality is sufficient. A decrease in current raises the efficiency at the cost of reduced power output. Hybridization with a micro-turbine and elimination of parasitic blower losses for this particular integration results in a similar net system output at considerably higher efficiency.

The changes to air flow, current, or fuel utilization necessary to operate the DFC-1500 in the compatibility window of the micro-turbine results in slightly different integrated system efficiencies, as summarized in Table 2.

It is important to note that without cathode recirculation the post-oxidizer cathode exhaust temperature is a function of operating temperature and the specific heating value only, as shown in Fig. 5. When designing from scratch the FC temperature may be known only within a certain range, allowing additional flexibility in the integration. However, most existing fuel cells are operated at a fixed temperature specified by the manufacturer and determined to provide the best performance with the least degradation and thermal stress. This results in a calculation of turbine inlet temperature that is solely a function of the specific fuel cell heating. The relationship can be seen to be nearly linear, but does in fact vary slightly with the inverse of voltage, which determines the ratio of electricity to heat production of the electrochemical reactions. Increasing current has the largest impact on voltage, and thus at

Table 2
Estimated efficiency of DFC-1500 hybridization.

Parameter	Nominal value	Changed value	System efficiency (%)	Air flow (kg s^{-1})
Air flow (ΔT)	132 °C	101 °C	68.5%	3.05
Fuel flow (U_{H2})	70%	85%	70.8%	2.60
Current	1400 A	1000 A	70.6%	2.03

Table 3
Capstone micro-turbine specification.

Specification	C-65	C-250	C-370 LP spool
Mass flow (lb/s)	1.08	3.44	3.2
Compressor outlet (F)	424	469	397
Compressor outlet (psig)	40	58.8	49
Recuperator outlet (F)	1050	1097	960
Turbine inlet (F)	1720	1788	1550
Efficiency (%)	31.2	33.25	34.5

low current densities the specific fuel cell heating is slightly higher for a given post-oxidizer temperature.

When both the fuel cell and micro-turbine have been specified by pre-existing equipment, the same hybrid system design methodology can be employed using non-scaled performance maps that are specific to each device. Without scaling, changes to the fuel cell operating conditions produce noticeably different trends compared to the case when the fuel cell size can be changed. On the other hand, the turbine performance map remains similar. The specification of the Capstone® line of micro-turbines is presented in Table 3, and the associated performance map shown in Fig. 6. The shaded region of Fig. 6 outlines the operating window for the C-250 turbine. Steady operation is achievable between 250 and 800 kW of total combustion heating, which produces between 50 and 250 kW of electric power. It is worthwhile to note that micro-turbines were found to exhibit poor emissions performance characteristics at low power during tests at UCI; however, this would not be an issue when hybridization replaces the combustor with clean electrochemical oxidation.

The DFC-1500® system nominally produces 1.4 MW after parasitic blower losses and inverter inefficiencies are considered. The fuel cell stack itself produces 1548 kWe of direct current power. The parasitic blower losses are typically eliminated by hybridization, but the inverter losses are not. Both have been removed in the performance map of Fig. 7. At first glance the DFC-1500® is substantially oversized for the C-250® engine, producing nearly 600 kW of excess total fuel cell heating under nominal conditions. The difference in scale is apparent in the specifications of each subsystem; the C-250 moves 3.4 lb s^{-1} of air while the DFC-1500 requires 5.1 lb s^{-1}. As discussed previously, several operating considerations could be manipulated to bridge the gap for hybridization.

Fig. 7 demonstrates the large impact that a fuel flow reduction has on the total fuel cell heating while minimally affecting the power output. Current proportionately reduces electric power and total fuel cell heating because as current is manipulated fuel flow

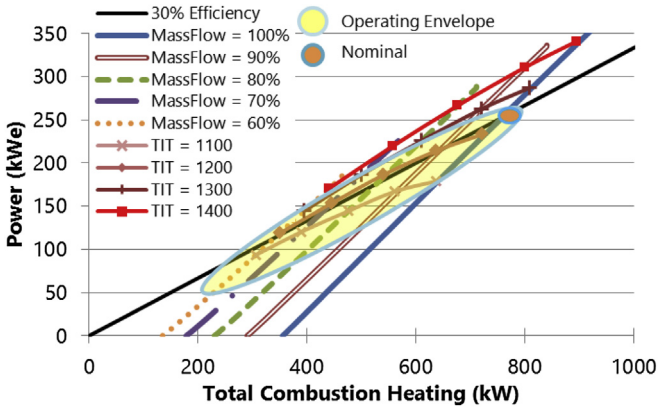

Fig. 6. Capstone(R) C-250 performance map.

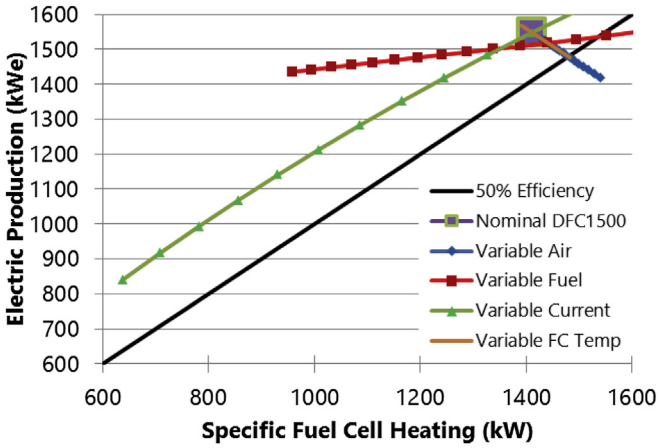

Fig. 7. DFC-1500® performance map comparing changes in air, fuel, and current flow.

rate was proportionally manipulated to maintain constant fuel utilization. A reduction of current without the associated reduction in fuel flow would reduce electric power and increase rather than decrease the specific fuel cell heating. A reduction in current from 1400 A to approximately 1050 A and a 34% reduction in fuel (increasing U_{H2} to 80%) would reduce the total fuel cell heating to 800 kW while producing ~1250 kWe. To determine the power output of the indirectly fired micro-turbine the achievable turbine inlet temperature must also be determined; see Fig. 5. The reduced air flow rate of the C-250 maintains the stack temperature rise, but the higher fuel cell efficiency (higher voltage) extracts more energy as electricity. Combined with the reduced fuel to air ratio, this lowers the achievable turbine inlet temperature to ~1000 K. Reflecting back to the C-250 map of Fig. 6 it can be seen that the maximum total combustion heating at 1000 K is 580 kW, which results in a MTG output of 150 kW. Combining the fuel cell and turbine power using Equation (4), the hybridized system would be able to produce 1400 kWe at 68.3% LHV efficiency before inverter losses. Further reduction in the operating current of the DFC-1500 would produce 1100 kWe and still generate 580 kW of total fuel cell heating at 1000 K; sufficient to fully replace the combustion heating and generate 150 kW in the MTG. Under these off-design conditions the hybridized system would produce 1250 kWe at 74.4% LHV efficiency. This ultra-high efficiency considers no heat losses from the fuel cell or inverter losses and perfect heat transfer to the turbine. Real systems would have lower efficiency because of these losses, but these results indicate that a hybrid system comprised of these components could produce ~1150 kWe at an efficiency approaching 70%.

4. SOFC–GT Topping cycle

The different attributes of the recuperated micro-turbines and large gas turbines suggest very different integrated hybrid cycles are necessary. Various concepts for the design of an SOFC–GT hybrid cycle appear in the literature. The particular cycle employed in this work, depicted in Fig. 8, was chosen for several reasons:

- Direct integration of the FC, rather than using an indirect heating method, eliminates the need for additional high temperature heat exchangers.
- Pressurization of the fuel cell increases performance
- Multiple bypass pathways and cathode recirculation allow for modulation of both the air flow rate and cathode inlet temperature for a fixed turbine rotational speed (which is required for some gas turbine sub-system designs).

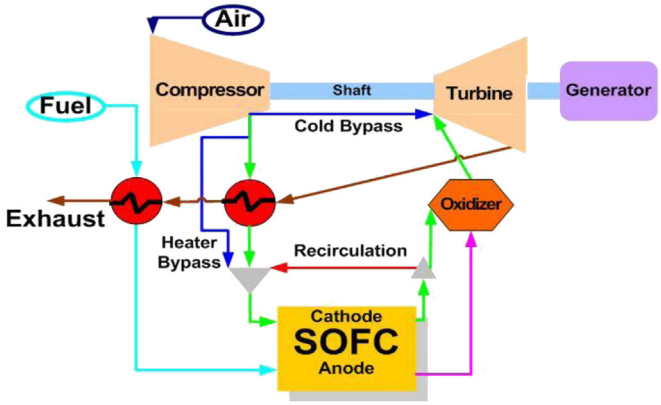

Fig. 8. SOFC–GT topping cycle configuration with axial flow turbine.

- Air compression provides pre-heating and increases the heat available to drive the turbine to produce additional electricity.

The drawbacks to this SOFC–GT topping cycle design include: (1) the directly coupled nature of the two generation devices, which requires rapid and sometimes advanced control algorithms, (2) the increased likelihood of cell fracture/damage due to pressurization and/or momentary pressure differences, and (3) increased likelihood of stall/surge due to the large volume of air within the cathode compartment (between the compressor and turbine).

The application of an SOFC–GT topping cycle ranges from the sub-MW scale distributed generation unit, to large 100-MW class generator units. The FC characteristics remain similar in both systems, with the pressurized SOFC producing upwards of 25% more power than that produced for atmospheric pressure operating conditions. The turbine and control characteristics differ with scale. At the sub-MW to multi-MW scale, integration of the turbo-machinery of a single stage radial-flow MTG is expected. The pressure ratio is limited to about 5 atm, and the compact nature of MTG turbo-machinery limits options for bypass loops. The MTG hybridization benefits from load-based rotational speed control that is typically already employed in the MTG design as a means of air flow rate manipulation, and the regenerative heater that is typically already incorporated to capture turbine exhaust energy. Axial flow turbines are larger, more efficient, employ additional control methods, and achieve substantially higher pressure ratios. Synchronous generation (constant shaft speed turbo-machinery) limits the means for air flow control to compressor bleed and inlet guide vane manipulation. The high pressure ratios achieved in modern multi-spool axial turbines (up to 60 atm for modern aero-derivative engines) can be reduced by removing the high pressure spool.

This section presents a power block design for a coal syngas fed SOFC combined with an axial flow turbine in a pressurized topping cycle. This system was selected to illustrate several distinctive characteristics that differ from the natural gas fueled MTG hybrid, and require different integration and control strategies. A MW or sub-MW class SOFC hybrid would likely be natural gas fed and the integration with a MTG would proceed similar to the MCFC discussed in the previous section. High temperature fuel cell systems are thermally integrated with the fuel processing unit which uses waste heat from the stack for the endothermic reactions which convert natural gas to hydrogen and carbon monoxide fuel stream used within the fuel cell. Without this heat sink the air flow requirement increases and the specific fuel cell heating decreases. For the natural gas fueled MCFC-radial-turbine hybrid, the fuel cell generated more than enough heat to drive the micro-turbine in systems with equal air flow requirements. The solution was to turn down the output of the MCFC. The syngas fueled SOFC-axial-turbine hybrid exhibits the opposite behavior, with the turbine requiring additional heating. Two possible solutions include cathode recirculation and post-anode firing of additional fuel in a combustor immediately upstream of the turbine. Both introduce an efficiency penalty on the system, but the penalty associated with recirculation is much less. This section will analyze the addition of cathode recirculation as it avoids the emissions associated with combustion and introduces an additional means of control for dynamic operation.

The primary differences between the axial and radial turbine are the regenerative heater and inlet guide vanes. The Capstone® micro-turbines presented previously employ variable speed generators to maintain high efficiency at reduced load by reducing the rotational speed. This reduces the air flow to maintain turbine exhaust temperature, and thus retains the same effectiveness in the regenerative heat exchanger. Because pressure ratio decreases with speed the turbine inlet temperature is lower despite the fixed exhaust temperature. This operating strategy causes the regeneration to provide a greater portion of the heat addition to the high pressure air, making the lower mass flow inherently more efficient as shown in Fig. 3.

The opposite is true for the axial flow turbine, which does not utilize a regenerative heat exchanger, and the specific combustion heating is much higher than a MTG. Since the SOFC-GT topping design of Fig. 8 includes a regenerative heat exchanger which transfers heat from the turbine exhaust to the cathode inlet, the performance map of Fig. 9 has been modified to represent an axial flow turbine with 200 °C of regenerative heat recovery. The heat recovery reduces the nominal specific combustion heating to approximately 125% of the nominal MTG combustion heating.

Axial flow turbines typically operate synchronously with the electric grid and employ inlet guide vanes rather than speed control to reduce the mass flow and maintain high operating temperatures for reduced load operating conditions. The guide vanes reduce the compressor efficiency and operating pressure, typically resulting in a substantial reduction of efficiency at reduced load. The achievable range of inlet guide vane manipulation without stalling the engine limits the operating regime of large turbine systems to typically between 70 and 100% of rated output. The wider operating range of a micro-turbine is more suitable to hybridization and load following control strategies.

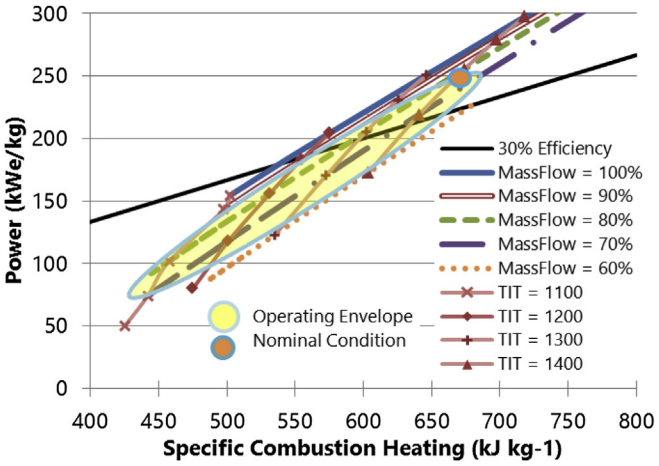

Fig. 9. Axial turbine performance map with exhaust heat recovery.

The SOFC performance map trends of Fig. 10 are similar to those of the MCFC. The syngas fuel eliminates the steam reformation cooling, increases the air flow requirement and results in much lower specific fuel cell heating. The SOFC voltage (consistent with U.S. Department of Energy targets) is slightly below that of a FuelCell Energy® DFC unit; thus, the nominal operation is slightly below 50% efficient. Because additional fuel injection does not provide stack cooling the air flow requirement is nearly the same at higher fuel flow rates. Some additional power is yielded due to the higher concentration of hydrogen in the anode compartment. The primary impact is additional heat release in the post-oxidizer and results in a more decoupled trend between power and heat release. The most important difference between the MCFC bottoming cycle and the SOFC topping cycle design is the capability to operate the solid state fuel cell at elevated pressure. Fig. 10 illustrates the advantage that elevated pressure has on stack performance. If one chooses to hold the operational power density constant, then operating voltage increases with increasing pressure. The relationship of current, air flow and operating temperature remain similar to that presented for the MCFC system. As in the MCFC case presented in Fig. 5, the post-oxidizer temperature is a function of only the average electrolyte temperature and the heat release rate value.

The regenerative heat exchanger is included in this system to increase the compatibility of axial turbines and a syngas fueled SOFC. It would likely be unnecessary for a natural-gas fueled SOFC. Without heat regeneration the specific combustion heating of an axial turbine ranges from 600 to 900 kJ kg^{-1}. The specific fuel cell heating of a syngas fueled SOFC ranges from 200 to 500 kJ kg^{-1}. This disparity requires cathode recirculation to act as a multiplier of the specific fuel cell heating. Cathode recirculation multiplies the effect of the specific fuel cell heating by changing the ratio of cathode air flow to turbine air flow from 1:1 to $(1-r)$:1; where r represents the proportion of cathode exhaust recirculated. Fuel cell bypass does the opposite, changing the mass flow ratio from 1:1 to 1:$(1-b)$; where b is the proportion of turbine air flow bypassed around the fuel cell.

The addition of a regenerative heat exchanger reduces the specific combustion heating by 200 kJ kg^{-1}, introducing some overlap in the operating envelopes of the two sub-systems. The integration could still benefit from the addition of cathode recirculation, despite the additional complexity. Cathode recirculation also changes the pre-heating requirement and introduces either a parasitic load if a blower is employed or a large pressure loss if an ejector is employed for the recirculation. Recirculating cathode exhaust provides a substantial amount of cathode inlet heating, replacing compression heating or heat exchange from elsewhere in the cycle. The pre-recirculation cathode temperature limits the compressor operating pressure unless some form of intercooling is applied. With a 750 °C SOFC operating temperature, 50% cathode recirculation, and a 200 °C temperature difference across the cathode, the pre-recirculation cathode inlet temperature would be 650 °C. Assuming standard atmospheric conditions and typical axial compressor efficiency of 82% the upper pressure limit for these hybrid system operating conditions becomes 15 atm.

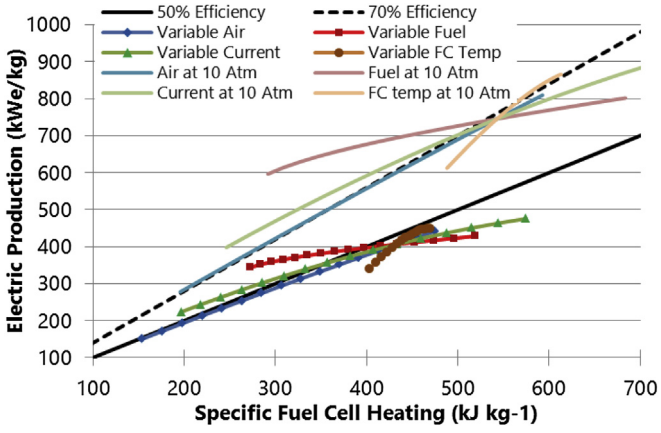

Fig. 10. SECA target SOFC operating on high hydrogen coal syngas at 1 and 10 atm.

4.1. Estimating efficiency with recirculation or bypass

With the additional complexity of cathode recirculation or fuel cell bypass the integration of these two performance maps is less straightforward. The "once through" air flow rates for the two devices will differ, thus a conversion factor, Equation (5), relates the specific fuel cell heating to the specific combustion heating it replaces. A simple modification to the previous efficiency estimate, shown in Equation (6), captures the impact of cathode recirculation. The post-oxidizer temperature estimate changes as recirculation increases, according to Equation (7). Similar expressions can be derived for fuel cell bypass which place a $(1-b)$ term in front of the fuel cell specific work and specific fuel cell heating. The estimate for the hybrid efficiency, Equation (6), does not consider the parasitic losses of a blower or ejector providing the recirculation. The blower parasitic can range from 1 to 3% of the nominal output depending upon the amount of recirculation and pressure drop across the fuel cell. Conveniently, Equation (5) can be re-arranged to estimate the recirculation necessary to achieve ideal thermal integration as $= 1 - \widehat{q}_{FC}/\widehat{q}_{GT}$.

$$\frac{\widehat{Q}_{GT}}{\dot{m}} = \frac{\widehat{Q}_{FC}}{(1-r)\dot{m}} \tag{5}$$

$$\eta_{hybrid} = \frac{w_{FC} + (1-r)w_{MGT}}{w_{FC} + \widehat{q}_{FC}} \tag{6}$$

$$T_{turbine\ inlet} = \frac{1}{(1-r)}(T_{oxidizer} - T_{cathode}) + T_{cathode} \tag{7}$$

Sample efficiency calculations are provided below using the nominal fuel cell condition at elevated pressure (750 kJ kg^{-1} electric and 550 kJ kg^{-1} of heat) and targeting the nominal turbine operation (250 kJ kg^{-1} electric and 670 kJ kg^{-1} heat). Using Equation (5) one determines that recirculation is 18% and Equation (6) yields an estimated hybrid efficiency of 73.5%. This quick approximation is quite close to (and slightly higher than) the 72.4% system efficiency calculated from a detailed simulation of this particular system that considers heat losses, heat exchanger ineffectiveness and the parasitic blower load. Application of this estimation method produced similar results for a variety of configurations and fuel cell types.

5. Discussion

Notice that in all of the integrated hybrid system designs investigated herein, there was typically a small operating window for the gas turbine, and a relatively large operating space for the fuel cell. The narrow operating envelope of current stand-alone fuel cell technology largely depends upon balance of plant constraints, while the stack itself may be substantially more flexible. The intersection of the stack and gas turbine operating envelopes outlines the region of feasible operation for

the hybrid system. Additional considerations such as stack longevity may limit the feasible operating temperatures and fuel utilizations. The introduction of cathode recirculation or bypass expands the hybrid operating envelope by changing the ratio of air flow between the two systems. It is to be expected that the operating window of both sub-systems will be diminished in a hybrid configuration, but through balance of plant design including recirculation, bypass, and supplemental combustors it is feasible to develop a hybrid with greater turn-down capability that either individual sub-system. The flame stability or emissions limits that constrain turbine operation near nominal are removed when hybridization replaces the combustion. The fuel cell, typically constrained by thermal integration with a fuel processor or air pre-heater, can also operate over a greater range of power with appropriate controls to manage cathode inlet temperature and flow rate. The second portion of this paper will elaborate on these controls which enable power tracking across a wide range.

Pressurization of the fuel cell is the primary advantage of an SOFC topping cycle due to the increased operating voltage and reduced air pre-heating requirement. At a pressure of 10 atm and constant power the voltage increases by 20% raising the efficiency and reducing current. Hybridization of a molten carbonate fuel cell with a micro-turbine in a bottoming cycle can achieve efficiencies >70% LHV, but requires a very close match between specific fuel cell heating and specific combustion heating, between post-anode oxidizer exhaust temperature and turbine inlet temperature, and between cathode and turbine air flow rates. Hybridization of a solid oxide fuel cell using coal syngas in a topping cycle requires cathode recirculation. With the addition of exhaust heat recovery the hybrid SOFC–GT can achieve 75% fuel to electric efficiency. A substantial difference between specific fuel cell heating and specific combustion heating can be accommodated with cathode recirculation or fuel cell bypass bringing the respective values of the two subsystems closer together.

6. Conclusions

This paper presented a novel methodology for pre-determining hardware compatibility for FC–GT hybridization that employs off-design performance maps generated from detailed, spatially resolved, physical component models. The methodology was able to uncover the underlying technical performance characteristics required for integration of hybrid FC–GT systems that led to the following conclusions.

- Without recirculation or bypass the specific fuel cell heating and specific combustion heating must closely match.
- Without recirculation or bypass the absolute flow rates of the turbine and fuel cell must match precisely.
- The total and specific combustion heating of an axial flow turbine can be greatly reduced with the inclusion of a regenerative heat exchanger
- Small changes in specific fuel cell heating can be achieved through changes in fuel flow, current, and thermal gradient
- The achievable post-oxidation temperature of the fuel cell must be within the suitable range of that required by the gas turbine.
  - The post-oxidation temperature of the fuel cell depends only upon the fuel cell operating temperature and the specific fuel cell heating.
- An estimation of the achievable system efficiency can be determined from the off-design operating envelopes of any fuel cell and turbine pair using Equation (4) or Equation (6).
- An over-sized turbine can be utilized with either pre- or post-FC fuel injection at the cost of reductions in hybrid system efficiency.
- An undersized turbine cannot be integrated with the fuel cell operating at full capacity. Higher efficiency may be achieved through de-rating the FC system but this design choice comes with the capital cost penalty of under-utilizing the fuel cell.

Acknowledgments

The authors gratefully acknowledge the financial support of the U.S. Department of Energy under contract number 09EE0001113 to the University of California, Irvine, which provided partial support for the research presented in this paper.

References

[1] W. Winkler, P. Nehter, M.C. Williams, D. Tucker, R. Gemmen, J. Power Sources (2006) 656–666.
[2] M.L. Ferrari, M. Pascenti, R. Bertone, L. Magistri, J. Fuel Cell Sci. Technol. 6 (3) (2009) 8, http://dx.doi.org/10.1115/1.3006200. Article 31008.
[3] D. Marra, B. Bosio, Int. J. Hydrogen Energy 32 (2007 January 8) 809–818.
[4] W.L. Lundburgh, S.E. Veyo, M.D. Moeckel, J. Eng. Gas Turbines Power (2003) 51–58.
[5] R. Roberts, J. Brouwer, J. Fuel Cell Sci. Technol. (2006) 18–25.
[6] D. McLarty, Y. Kuniba, J. Brouwer, S. Samuelsen, J. Power Sources 209 (2012 July) 195–203.
[7] M. Li, A.D. Rao, G.S. Samuelsen, Appl. Energy 91 (1) (2012) 43–50.
[8] M. Li, A.D. Rao, J. Brouwer, G.S. Samuelsen, J. Power Sources 195 (17) (2010) 5707–5718.
[9] M. Li, J. Brouwer, A.D. Rao, G.S. Samuelsen, J. Power Sources 196 (14) (2011) 5903–5912.
[10] S. Samuelsen, J. Brouwer, in: J. Garche (Ed.), Encyclopedia of Electrochemical Power Sources, first ed., Elsevier Science, 2009, pp. 124–134.
[11] A. Rao, J. MacLay, S. Samuelsen, J. Power Sources 134 (2004 June) 181–184.
[12] C. Howard, P. Oosthuizen, B. Peppley, Appl. Therm. Eng. 31 (2011) 2165–2170.
[13] A.S. Martinez, J. Brouwer, G.S. Samuelsen, J. Power Sources 213 (2012) 203–217.
[14] A.S. Martinez, J. Brouwer, G.S. Samuelsen, J. Power Sources 213 (2012) 358–374.
[15] T. Kaneko, J. Brouwer, G.S. Samuelsen, J. Power Sources (2006) 316–325.
[16] R.P.L. Bove, J. Power Sources 145 (2005 August 18) 588–593.
[17] F. Zabihian, A. Fung, Int. J. Eng. 3 (2) (2008) 85–119.
[18] M.C. Williams, J.P. Strakey, W.A. Surdoval, J. Power Sources 143 (2005) 191–196.
[19] Y. Zhao, N. Shah, N. Brandon, Int. J. Hydrogen Energy 36 (2011) 10235–10246.
[20] FuelCell Energy Inc, FCE Power Plant in Earth Day Dedication at Montana Clinic, Fuel Cells Bulletin, 2006 June 10.
[21] D. Tucker, M. Shelton, A. Manivannan, Electrochem. Soc. Interface 18 (3) (2009) 45–48.
[22] M. Ferrari, E. Liese, D. Tucker, L. Lawson, A. Traverso, Aristide Massardo, Trans. ASME (2007) 1012–1019.
[23] M.L. Ferrari, M. Pascenti, L. Magistri, A.F. Massardo, J. Fuel Cell Sci. Technol. 7 (2) (2010) 7, http://dx.doi.org/10.1115/1.3176663. Article 21005.
[24] M.L. Ferrari, A. Sorce, M. Pascenti, A.F. Massardo, Appl. Energy 88 (2011) 5090–5096.
[25] H. Ghezel-Ayagh, J. Walzak, D. Patel, J. Daly, H. Maru, R. Sanderson, W. Livingood, J. Power Sources 152 (2005) 219–225.
[26] J.H. Wee, Appl. Energy 88 (2011) 4252–4263.
[27] K.S. Oh, T.S. Kim, J. Power Sources 158 (2006) 455–463.
[28] D.P. Bakalis, A.G. Stamatis, Appl. Energy 103 (2013) 607–617.
[29] Y. Komatsua, S. Kimijima, J.S. Szmyd, Energy 35 (2010) 982–988.
[30] W.J. Yang, S.K. Park, T.S. Kim, J.H. Kim, J.L. Sohn, S.T. Ro, J. Power Sources 160 (2006) 462–473.
[31] W. Burbank, D. Witmer, F. Holcomb, J. Power Sources (2009) 656–664.
[32] A. Traverso, L. Magistri, A.F. Massardo, Energy 35 (2010) 764–777.
[33] T.W. Song, J.L. Sohn, T.S. Kim, S.T. Ro, J. Power Sources 158 (2006) 361–367.
[34] C. Stiller, Design, Operation and Control Modelling of SOFC/GT Hybrid Systems, Norwegian University of Science and Technology, Trondheim, 2006.
[35] F. Leucht, W.G. Bessler, J. Kallo, K.A. Friedrich, H. Müller-Steinhagen, J. Power Sources 196 (3) (2011) 1205–1215.
[36] J. Brouwer, F. Jabbari, E.M. Leal, T. Orr, J. Power Sources 158 (2005 November 14) 213–224.
[37] D. McLarty, J. Brouwer, G.S. Samuelsen, Int. J. Hydrogen Energy 38 (19) (2013) 7935–7946.
[38] P. Margalef, T. Brown, J. Brouwer, G.S. Samuelsen, Int. J. Hydrogen Energy (2011) 10044–10056.